Respiratory Physiology & Neurobiology 326 (2024) 104283

Contents lists available at ScienceDirect

Respiratory Physiology & Neurobiology

journal homepage: www.elsevier.com/locate/resphysiol

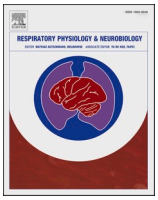

Estimation of differential pathlength factor from NIRS measurement in skeletal muscle

B. Koirala [b,i], A. Concas [a], A. Cincotti [a], Yi Sun [e,f], A. Hernández [h], M.L. Goodwin [i], L.B. Gladden [g], N. Lai [a,b,c,d,*]

[a] Department of Mechanical, Chemical and Materials Engineering, University of Cagliari, Italy
[b] Department of Electrical and Computer Engineering, Old Dominion University, Norfolk, VA, USA
[c] Biomedical Engineering Institute; Old Dominion University, Norfolk, VA, USA
[d] Department of Biomedical Engineering, Case Western Reserve University, Cleveland, OH, USA
[e] Key Laboratory of Adolescent Health Assessment and Exercise Intervention of Ministry of Education, East China Normal University, Shanghai 200241, China
[f] School of Physical Education & Health Care, East China Normal University, Shanghai 200241, China
[g] School of Kinesiology, Auburn University, Auburn, AL 36849, USA
[h] Faculty Research Liaison School of Social Sciences, Humanities and Arts University of California, USA
[i] Department of Orthopedic Surgery, Washington University, St. Louis, MO, USA

ARTICLE INFO

Edited by Dr. M Dutschmann

Keywords:
Heme group
Diffusion
Convection
Transport
Contraction
Hyperoxia
Modeling

ABSTRACT

The utilization of continuous wave (CW) near-infrared spectroscopy (NIRS) device to measure non-invasively muscle oxygenation in healthy and disease states is limited by the uncertainties related to the differential path length factor (*DPF*). *DPF* value is required to quantify oxygenated and deoxygenated heme groups' concentration changes from measurement of optical densities by NIRS. An integrated approach that combines animal and computational models of oxygen transport and utilization was used to estimate the *DPF* value *in situ*. The canine model of muscle oxidative metabolism allowed measurement of both venous oxygen content and tissue oxygenation by CW NIRS under different oxygen delivery conditions. The experimental data obtained from the animal model were integrated in a computational model of O_2 transport and utilization and combined with Beer-Lambert law to estimate *DPF* value in contracting skeletal muscle. A 2.1 value was found for *DPF* by fitting the mathematical model to the experimental data obtained in contracting muscle (T3) (Med.Sci.Sports.Exerc.48 (10):2013–2020,2016). With the estimated value of *DPF*, model simulations well predicted the optical density measured by NIRS on the same animal model but with different blood flow, arterial oxygen contents and contraction rate (J.Appl.Physiol.108:1169–1176, 2010 and 112:9–19,2013) and demonstrated the robustness of the approach proposed in estimating *DPF* value. The approach used can overcome the semi-quantitative nature of the NIRS and estimate non-invasively *DPF* to obtain an accurate concentration change of oxygenated and deoxygenated hemo groups by CW NIRS measurements in contracting skeletal muscle under different oxygen delivery and contraction rate.

1. Introduction

Near-Infrared spectroscopy (NIRS) can be used non-invasively to measure muscle oxygenation to evaluate physiological and pathophysiological conditions (Willingham and McCully, 2017; Grassi et al., 2019). The oxygenation of the heme group concentrations can be measured from different types of spectrometers: continuous wave (CW) NIRS provides concentration changes relative to a baseline; frequency domain (FD) or time domain (TD) NIRS provides absolute concentration (Ferrari et al., 2011; Grassi and Quaresima, 2016; Barstow, 2019).

The utilization of CW NIRS devices is limited by the uncertainties related to the differential path length factor (*DPF*) which is used in the Beer-Lambert law to quantify oxygenated ($\Delta HbMbO_2$) and deoxygenated ($\Delta HHbMb$) heme groups' concentration changes from the measurement of the optical density at different wavelengths. Thus, an incorrect *DPF* can lead to overestimate or underestimate the concentration changes (Endo et al. 2021; Pirovano et al. 2021). The typical range of values for *DPF* in brain and skeletal muscle tissues are:

* Corresponding author at: Department of Mechanical, Chemical and Materials Engineering, University of Cagliari, Italy.
E-mail address: nicola.lai@unica.it (N. Lai).

https://doi.org/10.1016/j.resp.2024.104283
Received 6 February 2024; Received in revised form 28 April 2024; Accepted 19 May 2024
Available online 22 May 2024

gastrocnemius (5.8–5.3), forearm (4.4–3.9), adult head (6.5–5.9) and infant head (5.4–4.7) (Ferrari et al. 1992; Duncan et al. 1995). It has been reported that *DPF* in tissues with a larger adipose tissue layer is higher for forearm and calf muscle (Ferrari et al. 1992; Duncan et al. 1995; Barstow, 2019). Thus, accurate *DPF* should be determined for each individual muscle group, taking into consideration the thickness of adipose tissue present (Pirovano et al. 2021), water content (Ferreira et al. 2007), and optical properties such as attenuation of light in the muscle due to absorption and scattering (Ferreira et al. 2007; Barstow, 2019; Endo et al. 2021; Pirovano et al. 2021). Besides the challenge related to the estimate of *DPF* which might in part be overcome with TD and FD NIRS spectrophotometers, the application of this technology is limited by the semi-quantitative nature of the signal obtained either with CW or TD and FD NIRS spectrophotometers. Specifically, the absolute or relative oxygenated ($HbMbO_2$) and deoxygenated ($HHbMb$) concentrations measured by NIRS devices result from the contribution of the oxygen content within an unknown microvascular and extravascular volume distribution. In addition, this volume distribution changes during exercise and it might be altered under disease states. Thus, the quantitative relationship between the NIRS signal and the heterogeneous oxygen distribution in the muscle region investigated is not known because a quantitative calibration of the signal *in vivo* is not available yet.

A quantitative approach based on a mathematical model of oxygen transport and metabolism has been proposed to quantify the contribution of Hb and Mb contribution to the NIRS signals (Koirala et al., 2021a, c, 2023; Lai et al., 2009). The analysis was based on concentration changes normalized to the changes from rest to ischemia because *DPF* was unknown. Nevertheless, this approach has not been applied to analyze absolute and relative concentration change measured by NIRS. We propose to use a physiologically based model of oxygen transport and utilization to relate optical density measured by NIRS to the oxygenated/deoxygenated heme group concentration changes in the microvascular (arteriole, capillary, venules) and extravascular compartments. To quantify this relationship the analysis was based on NIRS data obtained from a canine model of oxidative metabolism to avoid adipose tissue effects on the NIRS signals.

In this study, the computational model was used to: (1) estimate *DPF* using optical density measurements in pumped-perfused muscle at different blood flow rates; (2) predict muscle oxygenated and deoxygenated changes in independent experiments from those used to estimate *DPF*, and determine whether the optical density measured in these independent experiments were similar to those predicted by the simulations using the estimated *DPF*; and (3) analyze the effect of key physiological parameters on *DPF* estimation.

2. Methods

2.1. Animal model

The experimental data obtained from an animal model of oxidative metabolism reported in previous studies (Hernández et al., 2010b; Goodwin et al., 2012; Sun et al., 2016) were used to estimate and validate the *DPF*. It should be noted that the trial or experiment notation of this work is the same as that used in the experimental works (Hernández et al. 2010b; Goodwin et al. 2012; Sun et al. 2016) from which the NIRS data are used for the analysis proposed here (Table 1). The experimental protocol allows measurement of muscle venous oxygen (C^T_{ven}) concentration and optical density ($OD_{\lambda 1}$ and $OD_{\lambda 2}$) at two different wavelengths ($\lambda_1 = 760$ and $\lambda_2 = 860$ nm). All experimental data were averaged from 5 or 6 measurements for each trial condition. A continuous-wave NIRS system (Oxymon Mk III, Artinis Medical Systems BV) was used to measure the optical density ($OD_{\lambda 1}$ and $OD_{\lambda 2}$) associated with muscle oxygenation changes under different experimental conditions (i.e., blood flow, arterial O_2 content) and during contraction at different blood flows. The light at two different wavelengths (760 and 860 nm) was emitted and received by two fiber-optic bundles. The optodes were placed over the medial head of the left gastrocnemius and held in place with an elastic band. Experimental control of muscle blood flow was made possible by a peristaltic pump connected to the arterial inflow to the gastrocnemius. The right carotid artery or the right femoral artery was cannulated to route blood to the peristaltic pump (Hernández et al. 2010a).

Table 1
Experimental conditions of each trial.

Trial	Blood Flow	Contraction frequency (Metabolic rate)	Reference
B1 or B2	Self-perfused $\tau = 9$ *and* $17s$	0.66 Hz	(Hernández et al. 2010b)
CT20	Pump-perfused $\tau = 20s$	0.5 Hz	(Goodwin et al. 2012)
EX45	Pump-perfused $\tau = 45s$	0.5 Hz	(Goodwin et al. 2012)
EX70	Pump-perfused $\tau = 70s$	0.5 Hz	(Goodwin et al. 2012)
T3	Pump-perfused	0.5 Hz	(Sun et al. 2016)
T4	Pump-perfused	0.66 Hz	(Sun et al. 2016)

2.2. Mathematical model

A mathematical model of skeletal muscle oxygen transport and metabolism developed in another study (Koirala et al., 2021a, 2023) was used to estimate the *DPF* of the continuous wave NIRS used to measure the muscle oxygenation under different experimental conditions. The derivation of the equations to calculate the physiological variables of interest are based on previous models (Lai et al. 2007; Spires et al. 2012, 2013). The muscle volume (V_{mus}) is composed of extravascular tissue (cells and interstitial space, V_t) and blood (V_b) which is assumed to have vascular ($V_{b,v}$) and microvascular ($V_{b,m}$) compartments. The microvascular volume consists of arterioles, capillaries, and venules ($V_{b,m} = V_{art} + V_{cap} + V_{ven}$) with volume fraction ω_{art}, ω_{cap} and ω_{ven}.

The mathematical model simulates the spatial distribution of the free O_2 concentration in the capillary $C^F_{cap}(v)$ and extravascular $C^F_t(v)$ tissue compartments (Koirala et al. 2023). The concentrations depend on the tissue location as indicated by the muscle volume variable (v) from the arterial input $v = 0$ to the venous output $v = V_{mus}$. Also, the model quantifies the relationship between O_2 concentration dissolved (C^F) and bound (C^B) either to Hb (arterioles, capillaries, venules) or Mb (myocytes). These are used to quantify the oxygenated Hb (HbO_2) and Mb (MbO_2) concentrations in the microvascular and extravascular compartments of the muscle as:

$$HbO_2 = f_{b,m}\left[C^B_{art}\,\omega_{art} + C^B_{cap}\,\omega_{cap} + C^B_{ven}\,\omega_{ven}\right]\Big/4 = f_{b,m}(\Delta C^{\exp}_{Heme})\,C^B_{b,m}\Big/4 \quad (1)$$

$$MbO_2 = f_t\,C^B_t/4. \quad (2)$$

where $f_{b,m}$ and f_t are the microvascular and extravascular tissue volume fractions in muscle, $C^B_{b,m}$ is the bound O_2 concentration in the microvascular and C^B_{cap} and C^B_t are the spatial average of the bound O_2 concentration in capillary and extravascular tissue extravascular tissue (Koirala et al. 2023), respectively. $f_{b,m}$ is a function of the relative heme concentration changes ($\Delta C^{\exp}_{Heme}$) detected by the NIRS signal and used to quantify the microvascular volume changes. The bound concentration for blood and extravascular compartments is related to the dissolved

oxygen concentration by local equilibrium (Koirala et al. 2023). Similarly, the deoxygenated Hb (*HHb*) and Mb (*HMb*) contributions to the NIRS signal *HHbMb* are computed as:

$$HHb = f_{b,m}(\Delta C^{\exp}_{Heme})\ C_{b,Hb} - HbO_2 \tag{3}$$

$$HMb = f_t\ C_{t,Mb}/4 - MbO_2 \tag{4}$$

The derivation of the equations for interpreting the NIRS signal was documented in a previous human NIRS study (Lai et al., 2009). The simulated oxygenated and deoxygenated heme group concentrations of Hb and Mb relative to the rest condition (*R*) are calculated as:

$$\Delta HbO_2 = HbO_2 - HbO_2^R; \quad \Delta MbO_2 = MbO_2 - MbO_2^R \tag{5}$$

$$\Delta HHb = HHb - HHb^R; \quad \Delta HMb = HMb - HMb^R \tag{6}$$

Thus, the total oxygenated ($\Delta HbMbO_2$) and deoxygenated ($\Delta HHbMb$) heme group concentration changes relative to the resting conditions are then computed as:

$$\Delta HbMbO_2 = \Delta HbO_2 + \Delta MbO_2 \tag{7}$$

$$\Delta HHbMb = \Delta HHb + \Delta HMb \tag{8}$$

The total oxygenated ($HbMbO_2^R$) and deoxygenated ($HHbMb^R$) heme group concentration at rest were computed with the microvascular and extravascular volume distribution at rest (Table 2) by Eqs. (1)–(4).

Microvascular blood volume change. The oxygenated and deoxygenated NIRS measurements are integrated in the mathematical model to quantify microvascular blood volume changes (Koirala et al., 2021a) associated with the heme concentration changes detected by NIRS.

$$\Delta C^{exp}_{Heme} = \Delta HbMbO_{2\exp} + \Delta HHbMb_{\exp} = \Delta C^{mod}_{Heme} = \Delta C_{Hb} + \Delta C_{Mb} \tag{9}$$

The relative Hb and Mb concentration changes can be related to the microvascular blood volume fraction ($\Delta f_{b,m}$):

$$\Delta C_{Hb} = \Delta f_{b,m}\ C_{b,Hb};\ \Delta C_{Mb} = \frac{\Delta f_t\ C_{t,Mb}}{4} \tag{10}$$

$$\Delta C_{Hb} + \Delta C_{Mb} = \left(f_{b,m} - f^R_{b,m}\right) C_{b,Hb} + \frac{\left(f_t - f^R_t\right) C_{t,Mb}}{4} \tag{11}$$

$$\Delta C_{Hb} + \Delta C_{Mb} = \left(f_{b,m} - f^R_{b,m}\right)\left(C_{b,Hb} - C_{t,Mb}/4\right) \tag{12}$$

Combining Eq. (9) with Eq. (12) yields a relationship depending on $\Delta C^{\exp}_{Heme}$ measurement:

$$f_{b,m} = f^R_{b,m} + \frac{\Delta C^{exp}_{Heme}}{\left(C_{b,Hb} - C_{t,Mb}/4\right)} \tag{13}$$

The microvascular volume fraction in muscle at rest $f^R_{b,m}$ is calculated by the product of the blood volume fraction in muscle (f_b) and microvascular volume fraction in blood (f_m) at rest. Since $f_{b,m}$ changes are assumed to take place in capillaries, the volume change takes place in the microvascular compartment ($V_{b,m}$):

$$f_{b,m} = \frac{V_{b,m}}{V_t + V_{b,m} + V_{b,v}} \tag{14}$$

Table 2
Vascular, extravascular, and microvascular volume distribution at rest.

Notation	Description	Unit	Rest (R)
V_{mus}	Volume of muscle	[g]	62.5
f_b	fraction of systemic blood in muscle	[%]	7
f_t	fraction of tissue in muscle	[%]	93
f_m	fraction of microvascular blood in systemic blood	[%]	85
$f_{b,m}$	fraction of microvascular blood in muscle	[%]	5.95
ω_{art}	fraction of arterioles in microvascular blood	[%]	10

The $V_{b,m}$ change from rest (R) to each trial condition investigated is computed as:

$$V_{b,m} = V^R_{b,m} + \Delta V_{cap} = V^R_{b,m} + V_{cap} - V^R_{cap} \tag{15}$$

When blood volume changes occur, the extravascular (V_t), vascular ($V_{b,v}$), as well as arteriole (V_{art}) and venule (V_{ven}) volume remains constant at the resting value (See Table 2). Eqs. (14) and (15) can be rearranged as:

$$V_{cap} = \frac{f_{b,m}\ (V_t + V_{b,v})}{(1 - f_{b,m})} - \left[V^R_{b,m} - V^R_{cap}\right] = \frac{f_{b,m}\ (V_t + V_{b,v})}{(1 - f_{b,m})} - [V_{art} + V_{ven}] \tag{16}$$

Once the capillary volume is determined, the total microvascular volume can be calculated ($V_{b,m} = V_{art} + V_{cap} + V_{ven}$); thus, the arteriole, capillary, and venule volume fractions are:

$$\omega_{art} = \frac{V_{art}}{V_{b,m}}; \quad \omega_{cap} = \frac{V_{cap}}{V_{b,m}}; \quad \omega_{ven} = \frac{V_{ven}}{V_{b,m}} \tag{17}$$

The blood volume changes are attributed to the capillary compartment (V_{cap}), whereas arteriole and venule volumes are the same as those at rest and can be calculated from vascular, extravascular, and microvascular volume distribution (Table 2). The microvascular volume distribution was based on measurements from previous studies (Bebout, 1991; Hogan et al. 1993; Poole et al. 1995). $f_{b,m}$ is used to quantify V_{cap} and the arteriole, capillary, and venule volume fractions (ω_{art}, ω_{cap}, and ω_{ven}). Details to calculate the arteriole, capillary, and venule contributions to the NIRS signals are reported in our previous studies.

The reaction rate coefficient of the ATPase flux, k_{ATPase}, is a model parameter determined to simulate the NIRS signal for each trial (Table 1). The reaction rate coefficient can be computed as

$$k_{ATPase} = \frac{5.6\ VO_2}{f_t\ C_{ATP}} \tag{18}$$

where f_t is the extravascular tissue volume fraction in muscle and C_{ATP} is the concentration of ATP in muscle. Because the muscle oxygen uptake (VO_2) are available for only four muscle blood flow data, a regression line of the VO_2-Q data was used in Eq.(18) to calculate k_{ATPase} for each muscle blood flow of the simulations.

Estimate of DPF. For each physiological condition investigated, the simulated $\Delta HbMbO_2$ and $\Delta HHbMb$ concentrations are used to calculate the optical density with the modified Beer-Lambert law for Oxymon Mk III, Artinis Medical Systems BV as follows:

$$\Delta OD_{\mathrm{mod},\lambda 1} = \varepsilon_{HHbMb,\lambda 1}\cdot\Delta HHbMb\cdot d\cdot DPF + \varepsilon_{HbMbO_2,\lambda 1}\cdot\Delta HbMbO_2\cdot d\cdot DPF \tag{19}$$

$$\Delta OD_{\mathrm{mod},\lambda 2} = \varepsilon_{HHbMb,\lambda 2}\cdot\Delta HHbMb\cdot d\cdot DPF + \varepsilon_{HbMbO_2,\lambda 2}\cdot\Delta HbMbO_2\cdot d\cdot DPF \tag{20}$$

where, d is the source-detector distance, $OD_{\lambda 1}$ and $OD_{\lambda 2}$ are the optical density at two different wavelengths λ_1 and λ_2, respectively; $\varepsilon_{HbMbO_2,\lambda 1}$ (1.207 mM^{-1} cm^{-1}) and $\varepsilon_{HHbMb,\lambda 1}$ (0.798 mM^{-1} cm^{-1}) are the extinction coefficient for $HbMbO_2$ and $HHbMb$ at λ_1 and $\varepsilon_{HbMbO_2,\lambda 2}$ (0.761 mM^{-1} cm^{-1}) and $\varepsilon_{HHbMb,\lambda 2}$ (1.017 mM^{-1} cm^{-1}) are the extinction coefficients for $HbMbO_2$ and $HHbMb$ at λ_2. The optimal value of DPF is obtained by minimization of the least-square objective function:

$$f(DPF) = \sum_{i=1}^{n}\left(\Delta OD_{\exp,\lambda 1} - \Delta OD_{\mathrm{mod},\lambda 1}\right)^2_i + \left(\Delta OD_{\exp,\lambda 2} - \Delta OD_{\mathrm{mod},\lambda 2}\right)^2_i \tag{21}$$

where n indicates the number of experimental data. The minimization is accomplished by numerical optimization using the 'lsqcurvefit' library in MATLAB and imposing the user-defined constraints like lower and upper bounds. It should be noted that $\Delta OD_{\mathrm{mod},\lambda 1}$ e $\Delta OD_{\mathrm{mod},\lambda 2}$ are

calculated from Eqs. (19) and (20) whereas $\Delta HHbMb$ and $\Delta HbMbO_2$ are computed by the oxygen transport and utilization model Eqs. (7) and (8). The dependency of $\Delta HHbMb$ and $\Delta HbMbO_2$ from the oxygen concentration in the microvascular and extravascular compartments has been previously reported (Koirala et al. 2023).

Once the total oxygenated ($\Delta HbMbO_2$) and deoxygenated ($\Delta HHbMb$) heme group concentration changes are calculated from Beer-Lambert law for each time point, the absolute $HbMbO_2$ and $HHbMb$ concentrations can be estimated as follows:

$$HbMbO_2(t) = \Delta HbMbO_2(t) + HbMbO_2^R \tag{22}$$

$$HHbMb(t) = \Delta HHbMb(t) + HHbMb^R \tag{23}$$

The plots are used to visualize the comparison between experimental ($\Delta HbMbO_{2\text{exp}}$, $\Delta HHbMb_{\text{exp}}$) and simulated ($\Delta HbMbO_{2\text{mod}}$, $\Delta HHbMb_{\text{mod}}$) data for $\Delta HbMbO_2$ and $\Delta HHbMb$ obtained under different experimental conditions. Also, a quantitative comparison between simulated and measured value is quantified with the mean relative error (e) defined as:

$$e_{\Delta HbMbO_2} = \frac{\sum_{i=1}^{n}\left[\left(\Delta HbMbO_{2\text{exp}} - \Delta HbMbO_{2\text{mod}}\right)/\Delta HbMbO_{2\text{exp}}\right]_i}{n} \tag{24}$$

$$e_{\Delta HHbMb} = \frac{\sum_{i=1}^{n}\left[\left(\Delta HHbMb_{\text{exp}} - \Delta HHbMb_{\text{mod}}\right)/\Delta HHbMb_{\text{exp}}\right]_i}{n} \tag{25}$$

where n is the number of experimental data.

3. Results

3.1. DPF estimation

The DPF parameter value was estimated with the minimization of the objective function (Eq. (21)) based on the optical density measured and simulated by the mathematical model for different blood flows used in T3 trial. By fitting simulated optical density $OD_{\lambda 1}$ and $OD_{\lambda 2}$ to experimental data (Fig. 1a) obtained during different blood flow (T3), the optimal estimate was obtained for DPF (2.1) with a 95% confidence interval of (1.95, 2.21). As model input in these simulations, the parameter (k_{ATPase}) associated with the energy demand was used to simulate the changes in $V\dot{O}_2$ (Fig. 1b). With the estimated value of DPF, the oxygenated ($\Delta HbMbO_2$), deoxygenated ($\Delta HHbMb$) (Fig. 2a) and total heme (ΔC_{Heme}) group concentration changes (Fig. 2b) relative to rest condition were calculated. The oxygenated ($HbMbO_2$) and deoxygenated ($HHbMb$) heme group concentrations at rest were approximatively 240 and 7 μM, respectively. The total heme group concentration change was used to simulate the microvascular blood volume changes (Fig. 2c) by means of Eq. (13).

The capability of the mathematical model in reproducing the experimental data was checked by predicting the NIRS data for B1, B2, CT20, EX45, EX70, and T4 trails obtained at different blood flow rates (Q) during contraction (cf. Table 1). Specifically, for each condition the simulation to predict the optical density $OD_{\lambda 1}$ and $OD_{\lambda 2}$ (Fig. 3a), was obtained with the same set of parameter values including that of DPF whereas the parameter (k_{ATPase}) associated with the energy demand was used to simulate the changes in $V\dot{O}_2$ (Fig. 3b). The model predicted well the optical density $OD_{\lambda 1}$ and $OD_{\lambda 2}$ for each blood flow of all the investigated trials. The comparison between model simulations and experimental data was also reported in terms of oxygenated and deoxygenated NIRS signals as reported in Fig. 4. The concentration changes were obtained by converting the optical densities using the modified Beer-Lambert law. The model predicted well the changes of $\Delta HbMbO_2$ and $\Delta HHbMb$ (Fig. 4a) with O_2 delivery (Q) changes. The mean relative error ($e_{\Delta HbMbO_2}$, $e_{\Delta HHbMb}$) in predicting both the oxygenated and deoxygenated signals of B1, B2, CT20, EX45, EX70 and T4 experiments was approximately 16%. Model simulations tend to underestimate the experimental data for high blood flow. The higher the O_2 delivery, the lower the amplitude of the oxygenated and deoxygenated heme groups relative to the resting conditions. In both cases, the amplitude of $OD_{\lambda 1}$ decreased and $\Delta OD_{\lambda 2}$ increased slightly in response to an increase of O_2 delivery as shown in Fig. 3a.

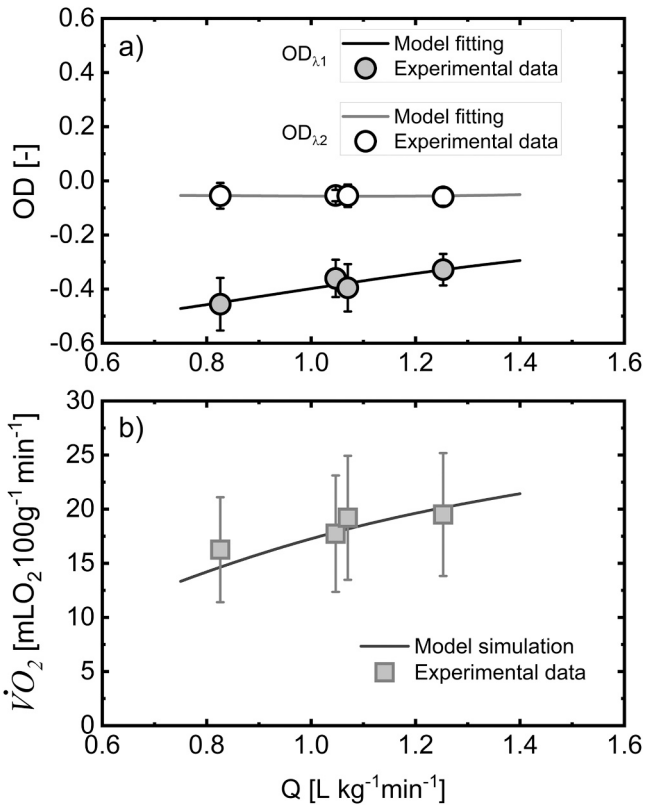

Fig. 1. Trial T3: comparison (a) between model fitting (solid line) and experimental data (open circles) for optical density ($OD_{\lambda 1}$ and $OD_{\lambda 2}$) and between model simulation and experimental data (grey squares) of muscle oxygen uptake ($V\dot{O}_2$) of trial T3 at different blood flow (Q).

3.2. Effect of microvascular blood volume on DPF

Because of the microvascular volume fraction $f_{b,m}$ variability and its changes during contraction (cf. Fig. 4c), we analyzed the effects of $f_{b,m}$ on the estimates of DPF as shown in Fig. 5: with a decrease of $f_{b,m}$ from 7% to 3.5%, the estimated value of DPF increased from 1.45 to 2.2. Experimental evidence showed that DPF is affected by blood volume changes.

4. Discussion

A mathematical model of muscle O_2 transport and metabolism was used to estimate the DPF for a constant wave NIRS instrument used to measure oxygenated and deoxygenated heme groups' concentration changes in skeletal muscle. With the estimated DPF, model simulations well predicted the optical density of NIRS data measured under different experimental conditions. This result demonstrates the capability of the model to quantify the NIRS data and relate it to O_2 transport and utilization conditions and suggests that the approach used can overcome the semi quantitative nature of the NIRS with sufficient information about the microvascular volume distribution at rest.

The estimate of DPF enables us to quantify the NIRS measurement in terms of absolute heme group concentration ($HbMbO_2$, $HHbMb$) in the whole skeletal muscle as a volume average of the extravascular and

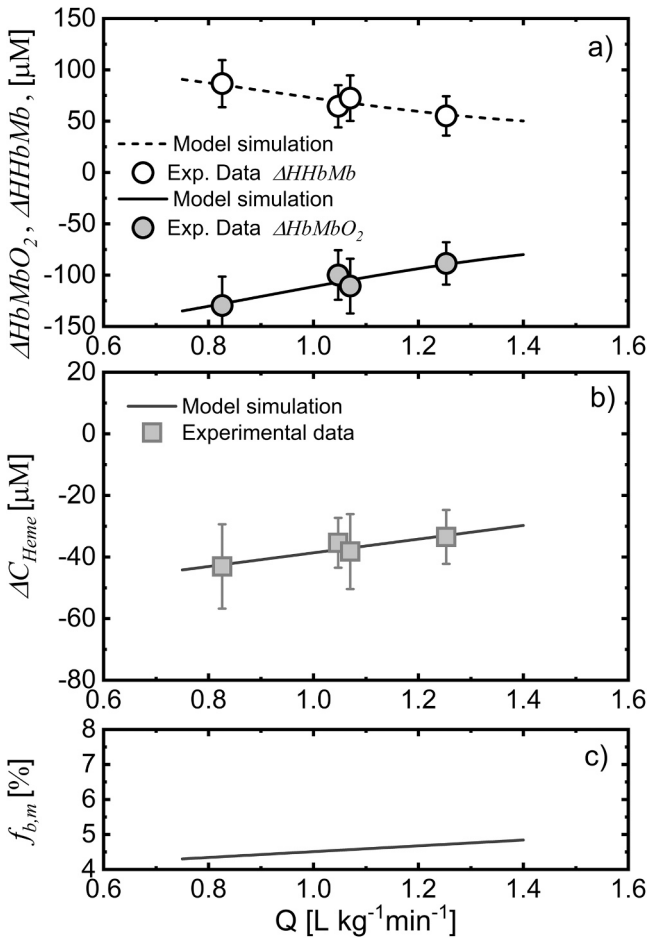

Fig. 2. Trial T3: comparison (a) between model simulation and experimental data (open and grey circles) for oxygenated ($\Delta HbMbO_2$) and deoxygenated ($\Delta HHbMb$) heme group concentrations changes, (b) heme group concentration changes (ΔC_{Heme}, grey squares) and (c) the microvascular volume fraction ($f_{b,m}$) changes with Q, $f_{b,m}$ is estimated from ΔC_{Heme} (Eq. (13)). The heme group concentrations changes are relative to the rest condition (R).

microvascular. The approach proposed in this work can be applied to NIRS measurement in human skeletal muscle with the knowledge of muscle blood flow. The estimate of DPF can be obtained by experiments designed to stimulate significant oxygenated and deoxygenated heme group concentration changes for blood flow at different workload.

4.1. Differential pathlength factor (DPF)

Besides the motion artifact related to the muscle contractions, the *DPF* is affected by the optical properties of the skeletal muscle including extravascular tissue (myocytes), adipose tissue, and blood volume. The *DPF* has been reported to be in the range between 4 and 6 and varies among different tissues (Chance et al. 1992). The *DPF* value (2.1) estimated in our work is lower than the values reported in the literature. In a human NIRS study, *DPF* for skeletal muscle was reported to be 4.3 (Ferrari et al. 1992). A possible difference between our *DPF* value and those reported in several studies could be related to the absence of adipose tissue in the skeletal muscle region investigated in our animal model because the NIRS probe was placed directly on the skeletal muscle. In support of this view, several studies reported a relationship between the adipose tissue layer and *DPF*. In a study on humans' vastus lateralis, *DPF* decreased linearly with a decrease of the adipose tissue thickness (Pirovano et al. 2021) and in the absence of adipose tissue, the *DPF* value is expected to be 2.6 which is close to that estimated in this work. Furthermore, another NIRS study on heart muscle reported a *DPF*

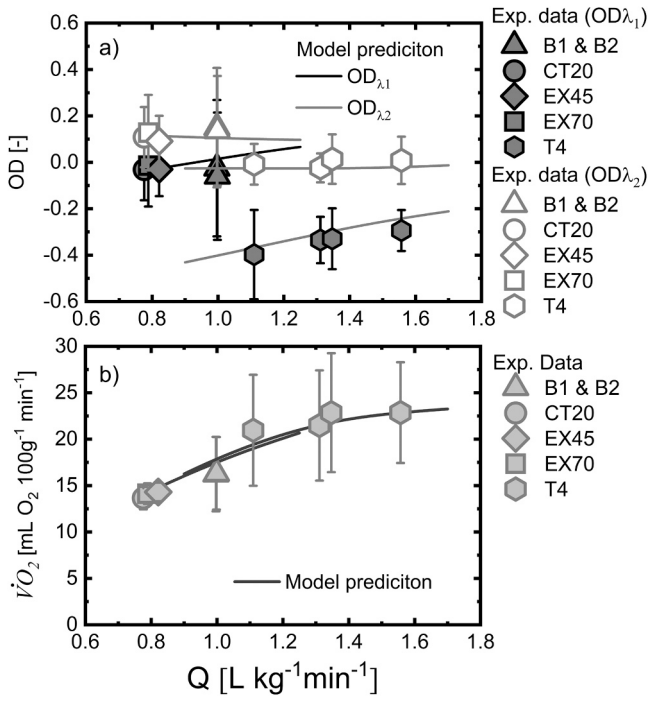

Fig. 3. Comparison between model prediction and experimental data for (a) optical density ($OD_{\lambda 1}$ and $OD_{\lambda 2}$) and comparison between model simulation and experimental data for muscle oxygen uptake ($\dot{V}O_2$) of the trials B1/B2, CT20, EX45, EX70 and T4 (Hernández et al. 2010b; Goodwin et al. 2012; Sun et al. 2016) for different blood flow (Q) during contraction.

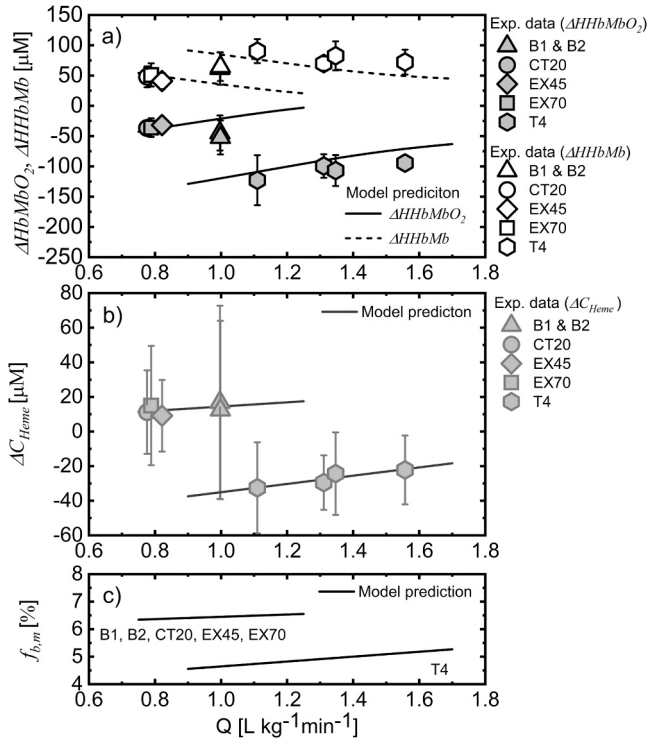

Fig. 4. Comparison between model prediction and experimental data for (a) oxygenated ($\Delta HbMbO_2$) and deoxygenated ($\Delta HHbMb$) heme groups concentration changes and (b) heme group concentration changes (ΔC_{Heme}) of the trials B1/B2, CT20, EX45, EX70 and T4 for different blood flow (Q) during contraction; and (c) the microvascular volume fraction ($f_{b,m}$) changes with Q estimated from ΔC_{Heme} (Eq. (13)). The heme group concentrations changes are relative to the rest condition (R).

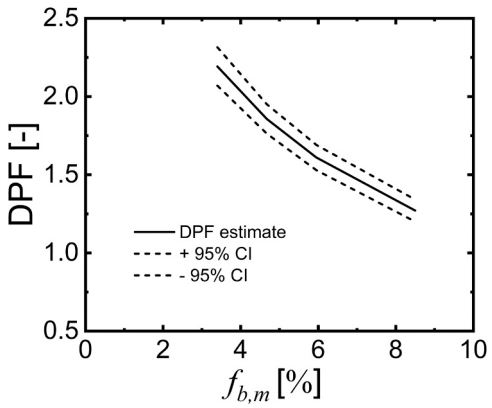

Fig. 5. Effect of microvascular volume on the estimation of DPF (solid line) and ± 95% confidence interval (short dash line).

range value of 1.8–4 (Nighswander-Rempel et al. 2005).

Uncertainty about the estimation of *DPF* is related to the microvascular volume distribution which was assumed to simulate the NIRS signals. Because *DPF* is particularly sensitive to $f_{b,m}$ (Fig. 5), even small variation of $f_{b,m}$ determined important changes in the estimate of *DPF*. Thus, our findings should be confirmed with more accurate evaluation of $f_{b,m}$, even though in our $f_{b,m}$ simulations we used values that are consistent and within the range reported in the literature. Existing experimental techniques such as MRI (Hindel et al. 2017) can be used to acquire quantitative information on the microvascular volume in skeletal muscle. The depth penetration of the light was not explicitly considered in our work. Usually, it is approximately half of the distance between the signal source and detector (Chance et al. 1992). Recently a statistical approach was proposed to provide a more accurate estimate of the penetration depth of light in media (Martelli et al. 2016). The error distribution for the data predicted in Fig. 4 presents an underestimation of the data value for high blood flow. Beside an error in the measurement, a possible reason for this discrepancy between simulated and measured data could be related to the uncertainties associated with the microvascular volume distribution. Indeed, the model predictions assume that the microvascular volume distribution is the same for all animal groups investigated. Although the animal groups present similar muscle characteristics, it is possible that among the groups the microvascular volume was different due to the probe position and group variability. Indeed, small changes in the microvascular volume can affect the *DPF* estimation (Fig. 5) and thus the NIRS signal.

Another important factor that could affect the estimate of *DPF* is the microvascular hematocrit which has been reported to be 50% (20–30%) of the systemic hematocrit (45–50%). In a NIRS study, this hematocrit has been considered to affect the NIRS signals (Davis and Barstow, 2013). Regardless of these current limitations in estimating *DPF*, it should be noted that the model can predict different experimental conditions with the same *DPF*, indicating that a unique *DPF* value is consistent with all NIRS measurements. The results of our simulations of the NIRS signal based on a volume average of the heme group concentration within the microvascular and extravascular compartments suggest that it is possible to overcome the semi-quantitative nature of the NIRS signal with accurate measurements of the microvascular blood volume fraction and distribution in skeletal muscles. Thus, a practical solution could be to determine the microvascular blood volume fraction by MRI at rest and use this information in the mathematical model to estimate *DPF* in contracting muscle.

Our NIRS experimental data were obtained assuming constant optical path length within the range of experimental conditions considered. It has been suggested that the optical path length varies during contraction; thus, the current assumption of considering a constant *DPF* would underestimate both NIRS signals (Endo et al. 2021). Further computational analysis could be performed with our mathematical model in combination with measurements of *DPF*.

4.2. Blood volume effect on DPF

The analysis of the NIRS data under different oxygen delivery conditions (Koirala et al., 2021a) indicated a primary role of capillary oxygen saturation in determining the sensitivity of the oxygenated and deoxygenated NIRS signal to blood volume change. Model simulations showed a decrease in *DPF* with an increase of microvascular blood volume. This finding is consistent with other experimental studies that reported a reduced optical path length with an increase in blood volume during exercise (Endo et al. 2021) or cuff occlusion (Ferrari et al. 1992; Hammer et al. 2019). In particular, for a blood volume increase of 28 μM detected by a Time-resolved NIRS during contraction, *DPF* decreased by 5–10% (Endo et al. 2021). Our analysis showed that an increase of microvascular volume corresponding to 8 μM determined a decrease in *DPF* of approximately 3%. Thus, the quantitative relationship between blood volume and *DPF* predicted by our model is close to that observed in this experimental study. Also, another human study attributed a *DPF* decrease of 7% to an increase in blood volume during cuff occlusion (Ferrari et al. 1992). The relative changes observed in these studies are consistent with those quantified by the mathematical model here proposed.

In conclusion, the integrative approach adopted allows us to estimate the *DPF* by relating the tissue oxygenation measurement by NIRS to the microvascular and extravascular volume distribution. This unique *DPF* can be used to quantify the oxygenated and deoxygenated heme group concentration changes from rest for different blood flow rates during contraction. This approach was further tested in predicting the oxygenated and deoxygenated heme group concentrations obtained with additional and independent experiments. This finding indicates that it is possible to quantify the heme group concentration measured by the NIRS device with reliable quantitative data on the microvascular and extravascular volume distribution within the muscle region investigated.

Author contributions

BK and NL contributed to the conception and design of the work. BK and NL integrated the experimental data to the model and run the simulations. All authors contributed to the analysis and interpretation of the data. BK and NL draft the manuscript. All authors read, revised, and approved the final version of the manuscript.

CRediT authorship contribution statement

Andres Hernández: Writing – review & editing, Formal analysis. **Matthew Goodwin:** Writing – review & editing, Formal analysis. **L. B. Gladden:** Writing – review & editing, Writing – original draft, Resources, Formal analysis. **Nicola Lai:** Writing – review & editing, Writing – original draft, Validation, Supervision, Software, Resources, Project administration, Methodology, Investigation, Funding acquisition, Formal analysis, Conceptualization. **Bhabuk Koirala:** Writing – review & editing, Writing – original draft, Validation, Methodology, Formal analysis, Conceptualization. **Alessandro Concas:** Writing – review & editing, Formal analysis. **Alberto Cincotti:** Writing – review & editing, Formal analysis. **Yi Sun:** Writing – review & editing, Formal analysis.

Declaration of Competing Interest

No conflicts of interest, financial or otherwise, are declared by the authors.

Data Availability

Data will be made available on request.

Acknowledgments

We thank Dr. A. Torricelli for providing thoughtful and constructive criticisms. This research was supported by National Institute of Arthritis and Musculoskeletal and Skin Diseases (NIH-NIAMS) under award number K25AR057206.

References

Barstow, T.J., 2019. Understanding near infrared spectroscopy and its application to skeletal muscle research. J. Appl. Physiol. 126, 1360–1376. https://doi.org/10.1152/japplphysiol.00166.2018.

Bebout D.E. (1991) The effect of exercise traning and immobilization on skeletal muscle gas exchange, capillary-fiber geometry and function-structure relationships.

Chance, B., Dait, M.T., Zhang, C., et al., 1992. Recovery from exercise-induced desaturation in the quadriceps muscles of elite competitive rowers. Am. J. Physiol. Cell Physiol. 262 https://doi.org/10.1152/ajpcell.1992.262.3.c766.

Davis, M.L., Barstow, T.J., 2013. Estimated contribution of hemoglobin and myoglobin to near infrared spectroscopy. Respir. Physiol. Neurobiol. 186, 180–187. https://doi.org/10.1016/j.resp.2013.01.012.

Duncan, A., Meek, J., Clemence, M., et al., 1995. Optical pathlength measurements on adult head, calf and forearm and the head of the newborn infant using phase resolved optical spectroscopy. Phys. Med. Biol. 40, 295–304.

Endo, T., Kime, R., Fuse, S., et al., 2021. Changes in optical path length reveal significant potential errors of muscle oxygenation evaluation during exercise in humans. Med. Sci. Sports Exerc 53, 853–859. https://doi.org/10.1249/MSS.0000000000002530.

Ferrari, M., Muthalib, M., Quaresima, V., 2011. The use of near-infrared spectroscopy in understanding skeletal muscle physiology: recent developments. Philos. Trans. R. Soc. A Math Phys. Eng. Sci. 369, 4577–4590. https://doi.org/10.1098/rsta.2011.0230.

Ferrari, M., Wei, Q., Carraresi, L., et al., 1992. Time-resolved spectroscopy of the human forearm. J. Photochem. Photobio. B 16, 141–153. https://doi.org/10.1016/1011-1344(92)80005-G.

Ferreira, L.F., Hueber, D.M., Barstow, T.J., 2007. Effects of assuming constant optical scattering on measurements of muscle oxygenation by near-infrared spectroscopy during exercise. J. Appl. Physiol. 102, 358–367. https://doi.org/10.1152/japplphysiol.00920.2005.

Goodwin, M.L., Hernández, A., Lai, N., et al., 2012. VO2 on-kinetics in isolated canine muscle in situ during slowed convective O2 delivery. J. Appl. Physiol. 112, 9–19. https://doi.org/10.1152/japplphysiol.01480.2010.

Grassi, B., Porcelli, S., Marzorati, M., 2019. Translational medicine: exercise physiology applied to metabolic myopathies. Med. Sci. Sports Exerc 51, 2183–2192. https://doi.org/10.1249/MSS.0000000000002056.

Grassi, B., Quaresima, V., 2016. Near-infrared spectroscopy and skeletal muscle oxidative function in vivo in health and disease: a review from an exercise physiology perspective. J. Biomed. Opt. 21, 091313 https://doi.org/10.1117/1.jbo.21.9.091313.

Hammer, S.M., Hueber, D.M., Townsend, D.K., et al., 2019. Effect of assuming constant tissue scattering on measured tissue oxygenation values during tissue ischemia and vascular reperfusion. J. Appl. Physiol. 127, 22–30. https://doi.org/10.1152/japplphysiol.01138.2018.

Hernández, A., Goodwin, M.L., Lai, N., et al., 2010a. Contraction-by-contraction VO2 and computer-controlled pump perfusion as novel techniques to study skeletal muscle metabolism in situ. J. Appl. Physiol. 108 https://doi.org/10.1152/japplphysiol.00963.2009.

Hernández, A., McDonald, J.R., Lai, N., Gladden, L.B., 2010b. A prior bout of contractions speeds Vo2 and blood flow on-kinetics and reduces the Vo2 slow-component amplitude in canine skeletal muscle contracting in situ. J. Appl. Physiol. 108 https://doi.org/10.1152/japplphysiol.01318.2009.

Hindel, S., Söhner, A., Maaß, M., et al., 2017. Validation of blood volume fraction quantification with 3D gradient echo dynamic contrast-enhanced magnetic resonance imaging in porcine skeletal muscle. PLoS One 12, 1–23. https://doi.org/10.1371/journal.pone.0170841.

Hogan, M.C., Bebout, D.E., Wagner, P.D., 1993. Effect of blood flow reduction on maximal O2 uptake in canine gastrocnemius muscle in situ. J. Appl. Physiol. 74, 1742–1747. https://doi.org/10.1152/jappl.1993.74.4.1742.

Koirala, B., Concas, A., Sun, Y., et al., 2021a. Blood volume versus deoxygenated NIRS signal: computational analysis of the effects muscle O2 delivery and blood volume on the NIRS signals. J. Appl. Physiol. 131, 1418–1431. https://doi.org/10.1152/japplphysiol.00105.2021.

Koirala, B., Concas, A., Sun, Y., et al., 2023. Relationship between muscle venous blood oxygenation and near-infrared spectroscopy: quantitative analysis of the Hb and Mb contributions. J. Appl. Physiol. 134, 1063–1074. https://doi.org/10.1152/japplphysiol.00406.2022.

Koirala, B., Saidel, G., Hernández, A., et al., 2021c. Effect of blood flow on hemoglobin and myoglobin oxygenation in contracting muscle using near-infrared spectroscopy. Adv. Exp. Med Biol. 1269 367–372.

Lai, N., Saidel, G.M., Grassi, B., et al., 2007. Model of oxygen transport and metabolism predicts effect of hyperoxia on canine muscle oxygen uptake dynamics. J. Appl. Physiol. 103, 1366–1378. https://doi.org/10.1152/japplphysiol.00489.2007.

Lai, N., Zhou, H., Saidel, G.M., et al., 2009. Modeling oxygenation in venous blood and skeletal muscle in response to exercise using near-infrared spectroscopy. J. Appl. Physiol. 106, 1858–1874. https://doi.org/10.1152/japplphysiol.91102.2008.

Martelli, F., Binzoni, T., Pifferi, A., et al., 2016. There's plenty of light at the bottom: Statistics of photon penetration depth in random media. Sci. Rep. 6 https://doi.org/10.1038/srep27057.

Nighswander-Rempel, S.P., Kupriyanov, V.V., Shaw, R.A., 2005. Assessment of optical path length in tissue using neodymium and water absorptions for application to near-infrared spectroscopy. J. Biomed. Opt. 10, 024023 https://doi.org/10.1117/1.1896372.

Pirovano, I., Porcelli, S., Re, R., et al., 2021. Effect of adipose tissue thickness and tissue optical properties on the differential pathlength factor estimation for NIRS studies on human skeletal muscle. Biomed. Opt. Express 12, 571. https://doi.org/10.1364/boe.412447.

Poole, D.C., Wagner, P.D., Wilson, D.F., 1995. Diaphragm microvascular plasma PO2 measured in vivo. J. Appl. Physiol. 79, 2050–2057. https://doi.org/10.1152/jappl.1995.79.6.2050.

Spires, J., Bruce Gladden, L., Grassi, B., et al., 2012. Model analysis of the relationship between intracellular PO2 and energy demand in skeletal muscle. Am. J. Physiol. Regul. Integr. Comp. Physiol. 303, R1110–R1126. https://doi.org/10.1152/ajpregu.00106.2012.

Spires, J., Gladden, L.B., Grassi, B., et al., 2013. Distinguishing the effects of convective and diffusive O2 delivery on VO2 on-kinetics in skeletal muscle contracting at moderate intensity. Am. J. Physiol. Regul. Integr. Comp. Physiol. 305, R512–R521. https://doi.org/10.1152/ajpregu.00136.2013.

Sun, Y., Ferguson, B.S., Rogatzki, M.J., et al., 2016. Muscle near-infrared spectroscopy signals versus venous blood hemoglobin oxygen saturation in skeletal muscle. Med Sci. Sports Exerc 48, 2013–2020. https://doi.org/10.1249/MSS.0000000000001001.

Willingham, T.B., McCully, K.K., 2017. In vivo assessment of mitochondrial dysfunction in clinical populations using near-infrared spectroscopy. Front. Physiol. 8, 1–11. https://doi.org/10.3389/fphys.2017.00689.